Insights into antiamyloidogenic properties of the green tea extract (−)-epigallocatechin-3-gallate toward metal-associated amyloid-β species

Suk-Joon Hyung[a], Alaina S. DeToma[a], Jeffrey R. Brender[a,b], Sanghyun Lee[c], Subramanian Vivekanandan[a,b], Akiko Kochi[a], Jung-Suk Choi[c,1], Ayyalusamy Ramamoorthy[a,b,2], Brandon T. Ruotolo[a,2], and Mi Hee Lim[a,c,2]

[a]Department of Chemistry, [b]Biophysics, and [c]Life Sciences Institute, University of Michigan, Ann Arbor, MI 48109

Edited by Harry B. Gray, California Institute of Technology, Pasadena, CA, and approved January 25, 2013 (received for review November 22, 2012)

Despite the significance of Alzheimer's disease, the link between metal-associated amyloid-β (metal–Aβ) and disease etiology remains unclear. To elucidate this relationship, chemical tools capable of specifically targeting and modulating metal–Aβ species are necessary, along with a fundamental understanding of their mechanism at the molecular level. Herein, we investigated and compared the interactions and reactivities of the green tea extract, (−)-epigallocatechin-3-gallate [(2*R*,3*R*)-5,7-dihydroxy-2-(3,4,5-trihydroxyphenyl)-3,4-dihydro-2*H*-1-benzopyran-3-yl 3,4,5-trihydroxybenzoate; EGCG], with metal [Cu(II) and Zn(II)]–Aβ and metal-free Aβ species. We found that EGCG interacted with metal–Aβ species and formed small, unstructured Aβ aggregates more noticeably than in metal-free conditions in vitro. In addition, upon incubation with EGCG, the toxicity presented by metal-free Aβ and metal–Aβ was mitigated in living cells. To understand this reactivity at the molecular level, structural insights were obtained by ion mobility-mass spectrometry (IM-MS), 2D NMR spectroscopy, and computational methods. These studies indicated that (*i*) EGCG was bound to Aβ monomers and dimers, generating more compact peptide conformations than those from EGCG-untreated Aβ species; and (*ii*) ternary EGCG–metal–Aβ complexes were produced. Thus, we demonstrate the distinct antiamyloidogenic reactivity of EGCG toward metal–Aβ species with a structure-based mechanism.

amyloid-β peptide | metal ions | natural products | amyloidogenesis

The brain of individuals with Alzheimer's disease (AD) has protein aggregates composed of misfolded amyloid-β (Aβ) peptides (1–4). The Aβ peptides are produced endogenously through enzymatic cleavage of amyloid precursor protein. Aβ monomers can misfold and oligomerize into various intermediates before the formation and elongation of fibrils that exhibit a characteristic cross–β-sheet structure (1–4). The accumulation of aggregated Aβ species has been a key feature of the amyloid cascade hypothesis, which cites that these aggregates are possible causative agents in AD. In addition, transition metals, such as Cu and Zn, whose misregulation leads to aberrant neuronal function, have a suggested link to AD pathology (1, 3–8). In vitro and in vivo studies have provided evidence for the direct interactions of metal ions with Aβ and their presence within Aβ plaques, indicating the formation of metal-associated Aβ (metal–Aβ) species. These metal–Aβ species have been implicated in processes that could lead to neurotoxicity (e.g., metal-induced Aβ aggregation and metal–Aβ-mediated reactive oxygen species generation) (1, 3–8). The involvement of metal–Aβ species in AD pathogenesis, however, has not been clearly elucidated. To advance our understanding of the potential neurotoxicity of metal–Aβ species, efforts to develop chemical tools capable of interacting directly with metal–Aβ species and modulating their reactivity in vitro and in biological systems are under way (1, 8–18). In particular, novel bifunctional compounds that contain elements for metal chelation and Aβ interaction have recently been prepared or identified via rational structure-based design strategies or systematic selection of natural products.

Naturally occurring flavonoids have been shown to interact with amyloidogenic peptides and arrest or redirect aggregation pathways (19–26). These studies have mainly been conducted under metal-free conditions. For example, the green tea extract, (−)-epigallocatechin-3-gallate [(2*R*,3*R*)-5,7-dihydroxy-2-(3,4,5-trihydroxyphenyl)-3,4-dihydro-2*H*-1-benzopyran-3-yl 3,4,5-trihydroxybenzoate; EGCG; Fig. 1*A*], is known as an antioxidative and anti-inflammatory agent for numerous human diseases (27) and has exhibited antiamyloidogenic reactivity with various disease-related peptides (e.g., Aβ, α-synuclein, islet amyloid polypeptide, semen-derived enhancer of virus infection) (19–21, 24, 25, 28–31). Nontoxic amorphous species were observed upon incubation of α-synuclein or Aβ with EGCG in the absence of metal ions, presumably through the direct peptide–EGCG interactions that were proposed to alter the peptide assembly from the expected fibrillar structures in favor of an off-pathway intermediate (20, 21). EGCG has also been shown to restructure preformed metal-free Aβ aggregates into unstructured, stable, and nontoxic conformations (21). These observations suggest a broad ability for EGCG to disrupt early-stage and late-stage aggregation processes. Although EGCG is also able to chelate metal ions (32, 33), its influence on metal-bound Aβ structure and reactivity has not been fully elucidated (34).

Here, we present the ability of EGCG to modulate metal [Cu(II) or Zn(II)]-induced Aβ aggregation to produce small, unstructured peptide aggregates to a different extent than metal-free Aβ aggregation, which may translate to reduced metal–Aβ toxicity in living cells. To rationalize the antiamyloidogenic reactivity of EGCG at the molecular level, Aβ interaction properties in the absence and presence of metal ions were investigated by ion mobility-mass spectrometry (IM-MS) (35, 36) and 2D NMR spectroscopy. Our IM-MS and 2D NMR results were also supported by molecular dynamics (MD) simulations to create a comprehensive molecular-level mechanism of EGCG action and reactivity. The interactions of EGCG with metal-free Aβ monomers and dimers induced structurally compact peptide conformations that likely led to the generation of amorphous Aβ

Author contributions: S.-J.H., A.S.D., J.R.B., A.R., B.T.R., and M.H.L. designed research; S.-J.H., A.S.D., J.R.B., S.L., S.V., A.K., and J.-S.C. performed research; S.-J.H., A.S.D., J.R.B., S.L., S.V., A.K., A.R., B.T.R., and M.H.L. analyzed data; and S.-J.H., A.S.D., J.R.B., A.R., B.T.R., and M.H.L. wrote the paper.

The authors declare no conflict of interest.

This article is a PNAS Direct Submission.

[1]Present address: Department of Chemistry, Cleveland State University, Cleveland, OH 44114.

[2]To whom correspondence may be addressed. E-mail: mhlim@umich.edu, bruotolo@umich.edu, or ramamoor@umich.edu.

This article contains supporting information online at www.pnas.org/lookup/suppl/doi:10.1073/pnas.1220326110/-/DCSupplemental.

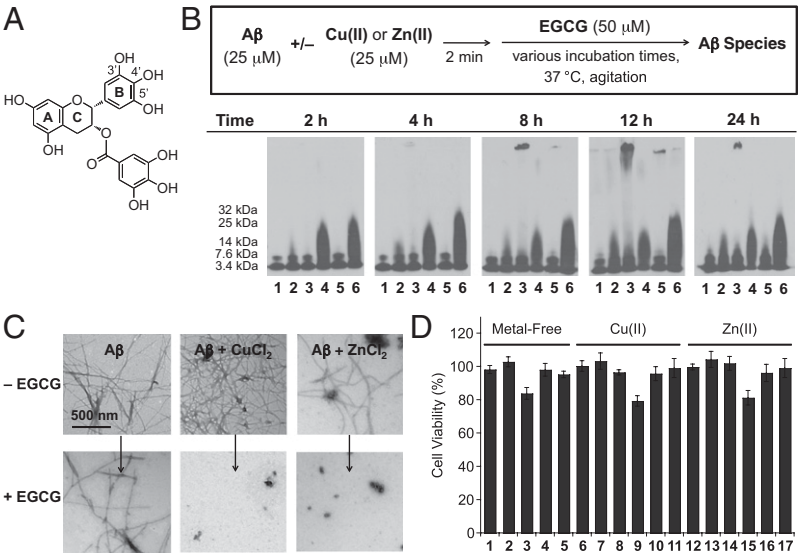

Fig. 1. Structure of EGCG (*A*), the assessment of its ability to modulate metal-free and metal-associated $A\beta_{1-40}$ aggregation in vitro (*B* and *C*), and the effect of EGCG on toxicity of $A\beta_{1-40}$ or metal–$A\beta_{1-40}$ species in living cells (*D*). (*A*) The letters A, B, and C identify the rings of the flavonoid core structure, and numbers indicate positions of OH groups. (*B*) Aβ species (from the inhibition experiment) visualized by gel electrophoresis using immunoblotting with an anti-Aβ antibody (6E10). Inhibition experiment (scheme, *Upper*): Aβ (25 μM) with or without $CuCl_2$ or $ZnCl_2$ (25 μM) were incubated with EGCG (50 μM) for 2, 4, 8, 12, or 24 h (pH 6.6 or 7.4; 37 °C; constant agitation). Lanes are as follows: 1, Aβ; 2, [Aβ + EGCG]; 3, [Aβ + $CuCl_2$]; 4, [Aβ + $CuCl_2$ + EGCG]; 5, [Aβ + $ZnCl_2$]; and 6, [Aβ + $ZnCl_2$ + EGCG]. (*C*) TEM images of the samples from *B* after 24 h incubation. (*D*) Cell viability measurements in the presence of metal-free and metal-treated Aβ species with or without EGCG in murine Neuro-2a neuroblastoma cells. Lanes are as follows: 1, EGCG (10 μM); 2, EGCG (20 μM); 3, Aβ (10 μM); 4, [Aβ + EGCG (10 μM)]; 5, [Aβ + EGCG (20 μM)]; 6, $CuCl_2$ (10 μM); 7, [$CuCl_2$ + EGCG (10 μM)]; 8, [$CuCl_2$ + EGCG (20 μM)]; 9, [Aβ (10 μM) + $CuCl_2$ (10 μM)]; 10, [Aβ + $CuCl_2$ + EGCG (10 μM)]; 11, [Aβ + $CuCl_2$ + EGCG (20 μM)]; 12, $ZnCl_2$ (10 μM); 13, [$ZnCl_2$ + EGCG (10 μM)]; 14, [$ZnCl_2$ + EGCG (20 μM)]; 15, [Aβ (10 μM) + $ZnCl_2$ (10 μM)]; 16, [Aβ + $ZnCl_2$ + EGCG (10 μM)]; and 17, [Aβ + $ZnCl_2$ + EGCG (20 μM)]. Cells treated with Aβ, metal ions, and/or EGCG were incubated for 24 h at 37 °C. Cell viability was measured by the MTT assay and viability was calculated relative to cells containing equivalent amounts of DMSO [0–1% (vol/vol)]. Error bars represent the SE from three independent experiments.

aggregates. In addition, our biophysical investigations for EGCG-treated metal–Aβ species imply the formation of ternary complexes, which may explain the remarkable ability of this molecule to influence metal-induced Aβ aggregation over the metal-free case. Overall, these studies provide a clear structure-based mechanism for EGCG action toward metal-free and metal-associated Aβ species and build a foundation for development and application of small molecules as chemical tools for elucidating AD pathogenesis.

Results and Discussion

EGCG Distinctly Modulates Aβ Aggregation Induced by Cu(II) or Zn(II). We investigated the ability of EGCG to inhibit the formation of metal-free or metal-associated $A\beta_{1-40}$ aggregates (inhibition experiment; Fig. 1 *B* and *C* and Fig. S1) or to disassemble preformed, aggregated species with or without metal ions (disaggregation experiments; Fig. S2) by gel electrophoresis with Western blotting using an anti-Aβ antibody (6E10), as well as by transmission electron microscopy (TEM). These methods were used to visualize the changes in size distribution and morphology that are not accurately represented by other biological assays [e.g., thioflavin-T (ThT) assay] (37, 38).

As shown in Fig. 1 *B* and *C* and Fig. S1 (inhibition experiment), EGCG displayed an enhanced ability to generate and stabilize low molecular weight (MW) Aβ aggregates when metal ions such as Cu(II) and Zn(II) were present. In comparison, only a modest amount of low-MW aggregates was detected at long incubation times in metal-free Aβ samples treated with EGCG (Fig. 1*B*, lane 2). Aggregates with a distribution of sizes [MW of ≤25 kDa or ≤32 kDa for EGCG-treated Cu(II)–Aβ or Zn(II)–Aβ species; Fig. 1*B*, lane 4 or 6] were observed even after only a 2- or 4-h incubation of Cu(II)- or Zn(II)-containing Aβ solutions with EGCG and were mostly maintained following a 24-h incubation. There was a slight dependence on the EGCG concentration for Cu(II)-treated Aβ species at the 4-h time point, at which smaller sizes of Aβ species (MW ≤ 25 kDa) could be produced even at substoichiometric conditions (e.g., 1:4:4 EGCG:Cu(II):Aβ; Fig. S1). TEM images showed that Aβ samples incubated with Cu(II) or Zn(II) and EGCG resulted in dramatic inhibition of the fibril formation process compared with those treated only with metal ions (Fig. 1*C*). In those systems, fibril growth was arrested, and the aggregates were observed to be smaller. Furthermore, the unstructured shapes of the aggregates were distinct from the fibrillar forms found in the metal–Aβ samples without EGCG (34); EGCG alone did not significantly change the morphology of metal-free Aβ species, which remained mostly long and fibrillar.

To investigate the effect of EGCG on transformation of aggregated Aβ forms (disaggregation experiment; Fig. S2), the compound was incubated with preformed, metal-free or metal-treated $A\beta_{1-40}$ aggregates for various time periods and analyzed by Western blotting and TEM. From these results, differences in aggregate distribution were detected for metal–Aβ samples compared with metal-free Aβ samples (Fig. S2*A*). The results for Cu(II)– or Zn(II)–Aβ indicated that even for short time periods (i.e., 2 or 4 h), a varied amount of low-MW (≤32 kDa) Aβ species was present. Cu(II)–Aβ aggregates treated with EGCG showed progressively weakening intensities in the Western blot at longer incubation times, whereas Zn(II)–Aβ aggregates treated with EGCG maintained a fairly constant level as time progressed. TEM analysis revealed some shorter fibrillar segments for EGCG-treated Cu(II)–Aβ, whereas the EGCG-treated Zn(II)–Aβ samples mainly produced amorphous species (Fig. S2*B*). Metal-free Aβ species incubated with EGCG partially retained fibrillar morphology, but some species were smaller in size than those observed in EGCG-untreated samples. Taken together, our results indicate that EGCG could discriminate between metal-free and metal-associated Aβ species driving the formation of low-MW aggregates at the expense of larger ones, demonstrating that the antiamyloidogenic behavior of EGCG is distinctive toward metal–Aβ species.

EGCG Diminishes Metal-Free and Metal–Aβ Toxicity in Living Cells. Previous studies have suggested that EGCG is able to alleviate toxicity of metal-free Aβ species in living cells (20, 21); however, a comparison of its influence on the toxicity of metal-free and metal–Aβ species has not been reported. Murine Neuro-2a neuroblastoma cells were used to probe the toxicity of EGCG, metal chloride salts (i.e., $CuCl_2$ and $ZnCl_2$), and/or $A\beta_{1-40}$ for 24 h (Fig. 1*D*). It was determined that EGCG (10 or 20 μM) with and without metal ions (10 μM) was relatively nontoxic to the living cells. In addition, the toxicity presented with metal-free

and metal-treated Aβ was negligible upon incubation with EGCG. Overall, these cell studies suggest that EGCG may mitigate the effect of metal-free or metal–Aβ-induced processes in complex, heterogeneous environments, through conformation alterations (20, 21, 24, 25, 34).

EGCG Directly Binds to Aβ Peptide and Causes Conformational Changes. To characterize the interactions between EGCG and $A\beta_{1-40}$, we first recorded 2D $^{1}H/^{15}N$ band-selective optimized flip-angle short transient (SOFAST)–heteronuclear multiple quantum correlation (HMQC) NMR spectra on samples with different molar ratios of EGCG in 25 mM Hepes, pH 7.3, with 25 mM NaCl at 4 °C (Fig. 2*A*). Under these conditions, the addition of EGCG to freshly dissolved $A\beta_{1-40}$ (76 μM) caused partial precipitation in the sample even with substoichiometric concentrations of EGCG to the peptide, suggesting EGCG could catalyze the production of aggregates from Aβ monomers. This precipitation was reflected in the SOFAST-HMQC spectra by a near-uniform decrease in intensity of all resonances of monomeric Aβ, most likely as a result of the depletion of Aβ monomers and enrichment of soluble and insoluble higher-order oligomers of Aβ (Fig. 2*A*).

To gain more insight into soluble oligomeric species invisible to NMR, IM-MS experiments were performed on samples with varying molar ratios of EGCG under conditions designed to probe their solution stoichiometry and structure (35, 36, 39). In the absence of EGCG, Aβ (10 μM) existed primarily as a mixture of monomers and dimers (Fig. 2*B*). The mass spectrum of Aβ contained peaks for the 4^+ and 3^+ states at 1,083 and 1,444 *m/z*, respectively. The formation of complexes between Aβ and EGCG was apparent from a solution containing Aβ (10 μM) and EGCG (20 μM; Fig. 2*C*). At this molar ratio, the signal corresponding to a complex composed of 1:1 stoichiometry was dominant in this dataset, as shown by the Aβ–EGCG complex in the 4^+ and 3^+ states at *m/z* of 1,198 and 1,597, respectively. Additional binding modes were also observed with ratios of 1:2, 2:1, and 2:2 Aβ/EGCG. Aβ dimers and their EGCG complexes were resolved in the 5^+ state at *m/z* 1,733, 1,824, and 1,916, respectively. The relative abundance of Aβ dimers was significantly increased in samples incubated with EGCG compared with Aβ samples without any additional molecules or with ThT (a fluorescent probe that binds to Aβ fibrils, but not monomers or small oligomers) (40) (Fig. 2*D*). This finding suggests that EGCG could facilitate the generation of soluble higher-order Aβ structures in solution, which was also supported through gel analysis of the samples prepared under conditions similar to the IM-MS experiment (Fig. S3). As shown in Fig. 2*D*, the gradual decrease of soluble dimeric Aβ species vs. monomeric Aβ species in the absence of EGCG or ThT was observed by IM-MS across time as an indication that dimeric species was likely depleted as a result of aggregation during lag phase of Aβ aggregate formation (41). Analysis of samples over 8 h, which was within the typical lag phase for Aβ of 8 to 18 h (42), was found to be complicated as a result of the formation of aggregates similar to those seen in the higher-concentration NMR sample that were likely unstable under our electrospray ionization conditions. Throughout this time interval, however, Aβ samples containing EGCG showed consistently higher levels of dimeric species, confirming that EGCG may promote and stabilize the formation of dimers.

IM-MS data also revealed the basis for a molecular-level explanation for the observed preference of EGCG for Aβ dimers over monomers (Fig. 2*C*). For $A\beta_{1-40}$ incubated with excess EGCG, IM arrival time distributions (ATDs) showed at least three resolved structural features, similar to previous data recorded for $A\beta_{1-42}^{3-}$ (43), allowing us to conformationally resolve distinct binding states. Binding of EGCG to Aβ shifted this distribution dramatically toward the most compact state [collision cross-section (CCS), centered at ~654 $Å^2$; Fig. 2*E* and Table S1]; additional binding of EGCG shifted this distribution even further toward more compact conformations (shorter drift time indicates more compact conformation). This change in the CCS distribution suggests that EGCG binding favors the generation of the most compact forms of the $A\beta_{1-40}$ monomer. Similarly, the soluble dimer bound to EGCG existed exclusively in a compact configuration, further supporting that formation of compact structural features was induced upon EGCG binding (Fig. 2*C*). Ion intensity values from mass spectra can be converted to EGCG K_d values given certain assumptions and careful experimental protocols (Table S2) (44). These measurements revealed that the affinity of EGCG for the dimeric forms of Aβ was higher than that for monomers [K_d values of 139 μM for 2:1 and 43.5 μM for 2:2 (Aβ dimer/EGCG) compared with of 331 μM for 1:1 and 47.1 μM for 1:2 (Aβ monomer/EGCG)]. These dissociation constants are in the range of previously reported K_d values, which varied based on temperature, concentration, and pH (45). The results imply that the collapse of Aβ monomer and dimer into more compact conformations following initial EGCG binding could facilitate additional EGCG binding. In addition, Aβ dimers likely have greater affinity for EGCG compared with monomers as a result of their preformed compact configuration compared with monomeric peptides, further suggesting that EGCG could bind to a region of the peptide

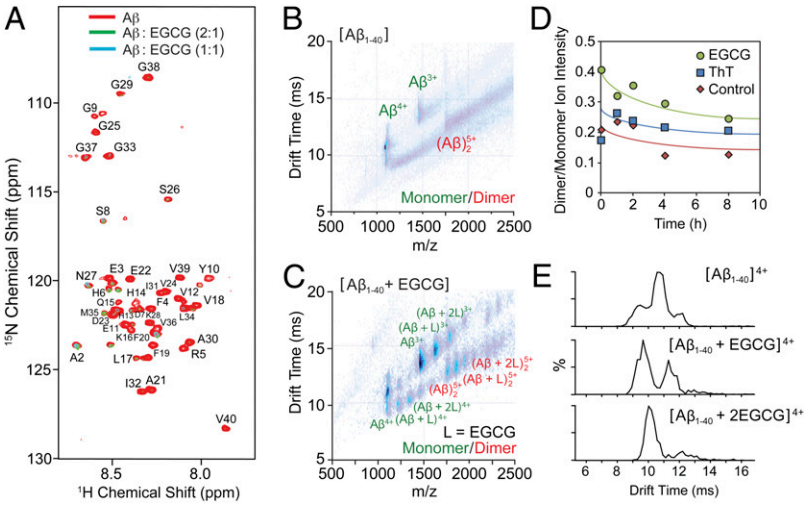

Fig. 2. Interaction of EGCG with $A\beta_{1-40}$. (*A*) Titration of Aβ with EGCG monitored by 2D $^{1}H/^{15}N$ SOFAST-HMQC NMR spectroscopy. Substoichiometric amounts of EGCG caused a large uniform decrease in intensity. (*B*) A plot of IM drift time vs. *m/z* for apo-$A\beta_{1-40}$ (10 μM) showed monomeric and dimeric forms of the peptide under conditions used for our experiments (100 mM ammonium acetate buffer, pH 7.4). (*C*) Similar IM-MS data as in *B* for samples containing EGCG added in solution (20 μM) revealed multiple binding modes for EGCG with the monomeric and dimeric form of Aβ. (*D*) MS-based time course experiments presented that EGCG (green circles) could solubilize larger amounts of the dimeric forms of the peptide in solution compared with ThT (blue squares) and only peptide (red diamonds; control). (*E*) Close inspection of the IM drift time profiles for the 4^+ state of the peptide indicated at least three resolved conformational families and that EGCG binding could produce a larger population of compact $A\beta_{1-40}$ peptides (CCS: 796, 716, and 633 $Å^2$, *Top* to *Bottom*; Table S1).

that does not participate in dimer formation. Thus, IM-MS and NMR results indicate that EGCG interacts with Aβ species, leading to their structural transformation to more compact configuration than that of apo-Aβ species.

Molecular Modeling Studies Present That EGCG Could Interact Directly with Aβ Monomer. To aid the interpretation of our IM-MS and NMR data, peptide-ligand docking studies were conducted against 10 structures of Aβ selected from a previously determined NMR structure of $Aβ_{1–40}$ (Protein Data Bank ID code 2LFM; Fig. S4) (46). According to the docking results, EGCG had a tendency to associate with Aβ primarily near the hydrophilic N-terminus and the α-helical region spanning residues H13 to D23 (46). This binding pocket is near the H6, H13, and H14 residues that may be responsible for metal binding to Aβ, as well as to residues in the hydrophobic self-recognition sequence, suggested to be linked to Aβ aggregation pathways (1, 3, 8, 47–49). A combination of polar (e.g., hydrogen bonding, electrostatic interaction) and hydrophobic interactions was likely responsible for the close proximity of EGCG to hydrophilic and hydrophobic portions of Aβ in solution. Furthermore, it appeared that the flexibility of EGCG was important in allowing the molecule to optimize several binding configurations with peptide and may be a contributing factor in its antiamyloidogenic properties (45).

MD simulations based on the 10 docked structures of the $Aβ_{1–40}$–EGCG complex determined above were carried out to identify the conformers observed in the experimental IM-MS data and explore structural elements involved in the Aβ–EGCG interaction (Fig. 3 and Figs. S5 and S6). Specifically, the docked structures were allowed to anneal by exposing the positively charged, desolvated Aβ–EGCG complex to a series of rapid heating and cooling cycles. For each starting structure, 100 structures were sampled at 300 K and their force field energy was recorded. In addition, the orientationally averaged CCS values were determined for these model structures by the trajectory method (50, 51). The plot of CCS against force field energy showed that the structures determined for Aβ–EGCG in the gas phase possess a diverse range of sizes, with CCS values ranging from 600 to 900 $Å^2$ (Fig. 3*A* and Fig. S5). Although the structures did not cluster to a narrow range of CCS or energy, we note that the docked conformation with the lowest binding energy led to structures with relatively smaller CCS values compared with those starting structures with less favorable binding energies (Fig. S6). Interestingly, Aβ simulated without EGCG occupied an even wider range of conformations than the previously described Aβ–EGCG complexes, as revealed by the broader distribution of CCS values computed for Aβ alone (Fig. 3*B*). In all cases, the experimentally determined values and trends were in good agreement with the MD results shown.

For those low-energy conformations whose CCS was close to the experimentally determined value of the compact structural feature of Aβ–EGCG complex, EGCG was slightly displaced from the residues considered to be associated with metal binding (H6, H13, and H14; Fig. 3*C*) (1, 3, 8, 47–49). By contrast, a select structure corresponding to a more extended conformation showed that EGCG was in proximity to those residues in similar manner to the docked pose (Fig. 3*D*). Gas-phase MD simulations led to significant perturbations in peptide secondary structure, but retained a helical motif region in the presence and absence of EGCG (Fig. 3 *C*–*E*). Similarly retained was the general binding location of the EGCG, which resided primarily between the central helical region and the N-terminus in all low-energy MD results that exhibited agreement with the IM-MS experiment. In all cases, the most favorable docked structures depicted in Fig. 3 provide the starting structures that generate the best-fit gas-phase structures for the IM-MS data. Moreover, the magnitude of the compaction observed in our IM-MS experiments was reproduced computationally in our MD simulations, revealing the interaction of EGCG with Aβ.

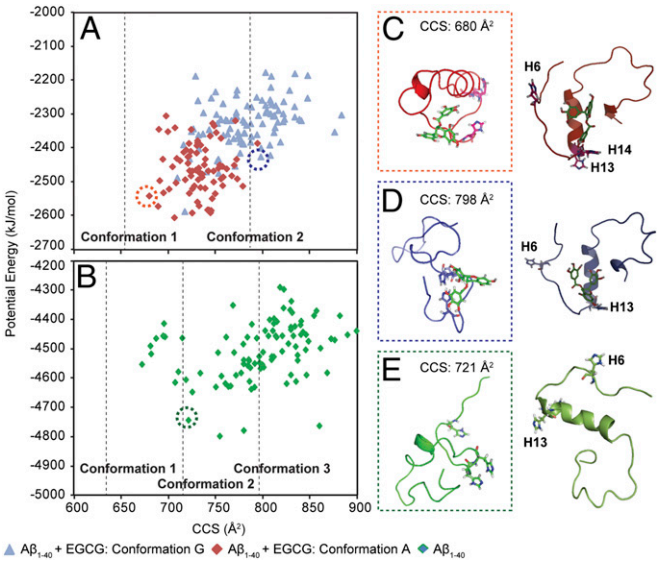

Fig. 3. Molecular modeling of EGCG-bound $Aβ_{1–40}$. (*A*) A plot of CCS against the potential energy of $Aβ_{1–40}$–EGCG complexes generated by MD simulation. Two binding states of the $Aβ_{1–40}$–EGCG complex (conformations 1 and 10) visualized by docking studies (Fig. S4) were subjected to a simulated annealing run, and 100 snapshots were sampled from the trajectory. (*B*) The corresponding run using the $Aβ_{1–40}$ monomer structure is shown (green diamonds). The values of CCS of the discrete conformations observed by IM-MS are marked as dotted lines. A representative gas-phase structure from the MD simulation (*Left*) with the corresponding starting structure (*Right*) are shown for the $Aβ_{1–40}$–EGCG complex with relatively low (*C*) and high (*D*) potential energy and (*E*) the $Aβ_{1–40}$ monomer (Protein Data Bank ID code 2LFM).

Metal Binding of EGCG Occurs in Absence and Presence of Aβ. In the framework of EGCG, OH groups found on the B ring and within the gallic acid moiety (Fig. 1*A*) could potentially be involved in Cu(II) and Zn(II) chelation (32, 33). In a pH 7.4 buffered aqueous solution, the UV-Visible (UV-Vis) absorption spectrum of EGCG (Fig. S7*A*) showed features *ca.* 275 nm and 320 nm, consistent with previous reports (33). The addition of 0.5 or 1 equivalent of $CuCl_2$ enhanced the absorption around 320 nm, possibly representing an assortment of complexes (32). Treatment of EGCG with 0.5 or 1 equivalent of $ZnCl_2$ also caused an optical change. Metal binding of EGCG in the presence of Aβ species was also investigated by UV-Vis spectroscopy (Fig. S7*B*). Optical bands from the samples containing Aβ, Cu(II) or Zn(II), and EGCG modestly resembled those from the samples in peptide-free conditions, indicating the possibility that EGCG has appropriate affinities for these metals in the presence of Aβ peptides.

EGCG Forms Ternary Complexes with Metal-Treated Aβ. To elucidate interactions of $Aβ_{1–40}$, EGCG, and Cu(II) or Zn(II), IM-MS and 2D NMR investigations were performed (Fig. 4). Mass spectra showed peaks corresponding to Cu(II)–Aβ species in 1:1 and 1:2 stoichiometries, and both types of Cu(II)–Aβ complexes bound to 1 or 2 equivalents of EGCG ([Aβ] = 10 μM; [Cu(II)] = 20 μM; Fig. 4 *A* and *B*).* IM data recorded for the monomeric Aβ

*It is worthwhile to note that the conditions in these experiments were not optimized for the formation of Aβ oligomers, and therefore the signal recorded for Aβ dimers and other oligomers at low abundance was insufficient to reveal the binding modes associated with higher-order Aβ or to determine the ligand binding constants associated with the tertiary complex (Fig. 4 *A* and *B*).

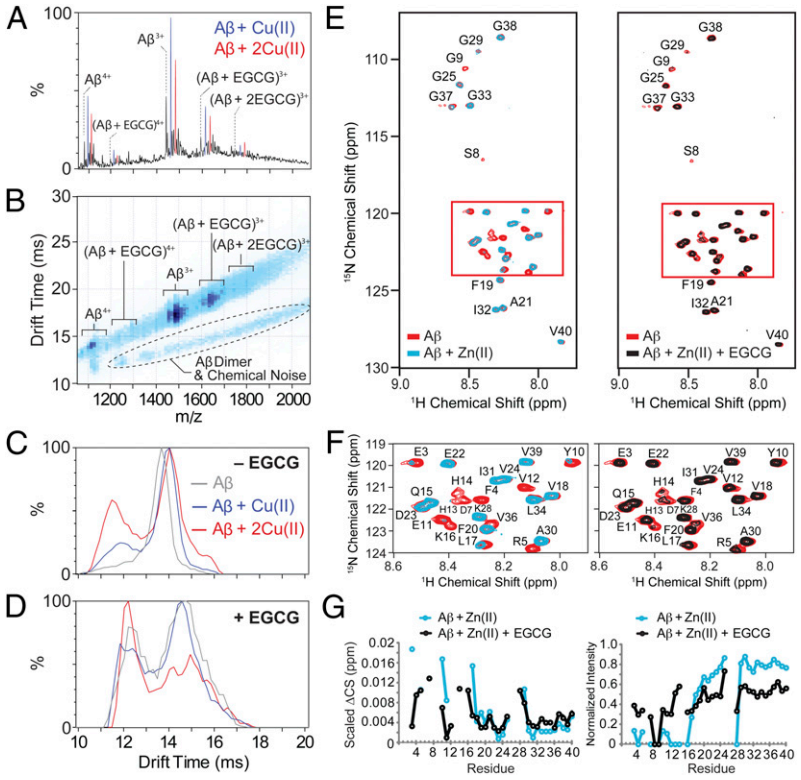

Fig. 4. Interactions of EGCG with metal–A$\beta_{1–40}$ species. (*A*) MS data for samples containing Aβ (10 μM), $Cu(OAc)_2$ (20 μM), and EGCG (20 μM) revealed the presence of ternary complexes. (*B*) A plot of IM drift time vs. *m/z* indicated that monomeric Aβ species generated in *A* followed one IM-MS trend, whereas higher-order Aβ complexes and chemical noise components were clearly distinguished from these signals by IM-MS. (*C*) IM drift time spectra for control data for which EGCG was not bound to the peptide revealed that Cu(II) binding acted to compact the peptide substantially. (*D*) Similar IM data as in *C* showed that EGCG–Cu(II)–A$\beta_{1–40}$ complexes further preferred compact configurations. (*E*) Analysis of EGCG and Zn(II) binding to A$\beta_{1–40}$ by 2D SOFAST-HMQC NMR spectroscopy at 4 °C. (*Left*) Addition of $ZnCl_2$ (38 μM) to Aβ (38 μM) caused the broadening and disappearance of specific peaks, primarily in the N-terminus. (*Right*) Subsequent addition of EGCG (38 μM) to the Zn(II)–Aβ complex partially restored the signal intensity. (*F*) Expanded view of the highlighted regions of the 2D NMR spectra (*E*). (*G*) Changes in the chemical shift (*Left*) and NMR signal intensity (*Right*) upon binding.

complexes showed that Cu(II) binding had a similar influence on $A\beta_{1–40}{}^{4+}$ as that observed for Aβ–EGCG complexes (Fig. 2), in that the most compact Aβ structures were the most favored upon binding either ligand individually or in combination. As presented in Fig. 4*C*, Cu(II) binding caused the peptide to favor the most compact of the three conformational families observed in apo-Aβ datasets, and such structural features became more pronounced in IM ATD profiles upon additional Cu(II) binding. Likewise, IM ATDs acquired for ternary complexes, involving EGCG, Cu(II), and Aβ, exhibited that the relative abundance of compact structural conformations was augmented for higher-stoichiometry Cu(II) to Aβ–EGCG complexes (Fig. 4*D*). The structural compaction of Cu(II)–Aβ even with EGCG suggests that Cu(II) could interact with Aβ in a noncooperative manner.

Under the same conditions as the experiments of Cu(II)–Aβ described earlier, IM-MS analysis of Zn(II) with A$\beta_{1–40}$ showed weaker association, even in the presence of excess Zn(II) (Fig. S8). Thus, to understand the interaction of EGCG with Zn(II)-treated A$\beta_{1–40}$ species, we first examined freshly dissolved A$\beta_{1–40}$ in the presence of Zn(II) alone by 2D SOFAST-HMQC NMR. The addition of $ZnCl_2$ to A$\beta_{1–40}$ at a 1:1 molar ratio broadened and shifted resonances for the region around H6, H13, and H14, previously identified as the primary Zn(II) binding site in the peptide (Fig. 4 *E*–*G*) (1, 3, 8, 47–49). The C-terminal region of the peptide (L17–V40) was mostly unaffected, except for the K28 and G29 resonances, which were significantly broadened or shifted, respectively, upon treatment with Zn(II). The reasons for changes in this region of the peptide are not immediately clear; however, the C-terminus is involved in contacts with central hydrophobic core (46), and there is evidence that Zn(II) affects this interaction (48). Addition of 1 equivalent of EGCG to this sample of Aβ and Zn(II) largely reversed the broadening and chemical shift changes for most of the peptide residues influenced by introduction of Zn(II) (Fig. 4 *E*–*G*). Among the residues that were not completely restored were H13 and H14, which have been identified as ligands in Zn(II) binding to Aβ (1, 3, 8, 47–49). This may imply that some amount of Zn(II) remains associated with Aβ whereas the remainder is displaced from its N-terminal binding site in Aβ by EGCG. Alternatively, the partial restoration of the resonance could represent the formation of a ternary complex of EGCG–Zn(II)–Aβ, as seen for the EGCG–Cu(II)–Aβ complexes studied by IM-MS. Finally, a combination of metal chelation/displacement by EGCG and ternary complex generation could occur simultaneously. Overall, our studies suggest that EGCG is able to interact with Cu(II)– or Zn(II)–Aβ species directly, likely leading to generation of ternary complexes with metal-associated Aβ, which may account for its antiamyloidogenic reactivity with metal–Aβ species (Fig. 1 and Figs. S1–S3).

Summary. The green tea extract EGCG, which has a structure capable of metal chelation and Aβ interaction, was selected as a scaffold to examine the reactivity of a well known natural flavonoid with metal-free and metal-associated Aβ species and to provide structure-based insights into its mode of action at the molecular level. It was observed that addition of EGCG to samples containing Cu(II)– or Zn(II)–Aβ species produced small amorphous Aβ aggregates, whereas EGCG-untreated samples generated mainly structured Aβ aggregates. This reactivity with Aβ was more noticeable in conditions containing metal ions, suggesting that EGCG was more capable of disrupting metal-mediated Aβ aggregation pathways compared with metal-free conditions. Furthermore, in living cells, incubation of EGCG with metal-free or metal–Aβ enhanced cell survival, which may represent its inhibitory effect on aggregation in complex settings. Our IM-MS and NMR results suggest that the overall mechanism of reactivity of EGCG with metal-free and metal-associated Aβ species could be driven by its ability to influence the structure of Aβ monomers and dimers [i.e., formation of more compact conformations of Aβ and/or ternary complexes containing Aβ, Cu(II) or Zn(II), and EGCG in multiple stoichiometries]. Taken together, the natural product, EGCG, could modulate the reactivity (i.e.,

aggregation, toxicity) of metal–Aβ species through direct interactions with the peptide and its metal complexes. In addition, the molecular-level insights that underlie this altered reactivity suggest that EGCG might generate off-pathway Aβ intermediates preferentially in the presence of metal ions. Thus, the fundamental information on the structure–interaction–reactivity relationship presented here will undoubtedly aid in rational design and structure-based screening strategies to identify chemical tools to elucidate the contributions of multiple and/or interconnected factors in AD pathogenesis.

Materials and Methods

$A\beta_{1-40}$ was purchased from Anaspec. EGCG was purchased from Sigma-Aldrich and used without further purification. Mass spectra were acquired on a quadrupole IM time-of-flight mass spectrometer (Synapt G2 HDMS; Waters) and LCT Premier mass spectrometer fitted with a nano-electrospray ionization source (Waters). The NMR investigations were conducted on a 600-MHz Bruker spectrometer equipped with a cryogenic probe at 4 °C. More detailed experimental descriptions are included in *SI Materials and Methods*.

Note. During the review process of our studies, a paper regarding the influence of EGCG on Aβ aggregation in the presence of metal ions monitored by surface plasmon resonance imaging (SPRi) was published (34). Differences in Aβ fibril formation were reported in the absence and presence of metal ions and EGCG using SPRi. Samples containing EGCG produced less SPRi intensity, suggesting its ability to alter fibril formation in favor of producing unstructured aggregates.

ACKNOWLEDGMENTS. This work was supported by National Institutes of Health Grants GM-084018 (to A.R.) and GM-095832 (to B.T.R.), Alzheimer's Association New Investigator Research Grant NIRG-10-172326, the Alzheimer's Art Quilt Initiative, American Heart Association (to M.H.L.), and a Graduate Research Fellowship from the National Science Foundation (to A.S.D.).

1. DeToma AS, Salamekh S, Ramamoorthy A, Lim MH (2012) Misfolded proteins in Alzheimer's disease and type II diabetes. *Chem Soc Rev* 41(2):608–621.
2. Ross CA, Poirier MA (2004) Protein aggregation and neurodegenerative disease. *Nat Med* 10(Suppl):S10–S17.
3. Kepp KP (2012) Bioinorganic chemistry of Alzheimer's disease. *Chem Rev* 112(10): 5193–5239.
4. Jakob-Roetne R, Jacobsen H (2009) Alzheimer's disease: From pathology to therapeutic approaches. *Angew Chem Int Ed Engl* 48(17):3030–3059.
5. Crouch PJ, Barnham KJ (2012) Therapeutic redistribution of metal ions to treat Alzheimer's disease. *Acc Chem Res* 45(9):1604–1611.
6. Que EL, Domaille DW, Chang CJ (2008) Metals in neurobiology: Probing their chemistry and biology with molecular imaging. *Chem Rev* 108(5):1517–1549.
7. Eskici G, Axelsen PH (2012) Copper and oxidative stress in the pathogenesis of Alzheimer's disease. *Biochemistry* 51(32):6289–6311.
8. Pithadia AS, Lim MH (2012) Metal-associated amyloid-β species in Alzheimer's disease. *Curr Opin Chem Biol* 16(1-2):67–73.
9. Rodríguez-Rodríguez C, Telpoukhovskaia M, Orvig C (2012) The art of building multifunctional metal-binding agents from basic molecular scaffolds for the potential application in neurodegenerative diseases. *Coord Chem Rev* 256(19-20):2308–2332.
10. Braymer JJ, DeToma AS, Choi J-S, Ko KS, Lim MH (2011) Recent development of bifunctional small molecules to study metal-amyloid-β species in Alzheimer's disease. *Int J Alzheimers Dis* 2011:623051.
11. Perez LR, Franz KJ (2010) Minding metals: Tailoring multifunctional chelating agents for neurodegenerative disease. *Dalton Trans* 39(9):2177–2187.
12. Pithadia AS, et al. (2012) Reactivity of diphenylpropynone derivatives toward metal-associated amyloid-β species. *Inorg Chem* 51(23):12959–12967.
13. Sharma AK, et al. (2012) Bifunctional compounds for controlling metal-mediated aggregation of the $A\beta_{42}$ peptide. *J Am Chem Soc* 134(15):6625–6636.
14. Choi J-S, Braymer JJ, Nanga RPR, Ramamoorthy A, Lim MH (2010) Design of small molecules that target metal-Aβ species and regulate metal-induced Aβ aggregation and neurotoxicity. *Proc Natl Acad Sci USA* 107(51):21990–21995.
15. Braymer JJ, et al. (2011) Development of bifunctional stilbene derivatives for targeting and modulating metal-amyloid-β species. *Inorg Chem* 50(21):10724–10734.
16. Rodríguez-Rodríguez C, et al. (2009) Design, selection, and characterization of thioflavin-based intercalation compounds with metal chelating properties for application in Alzheimer's disease. *J Am Chem Soc* 131(4):1436–1451.
17. Hindo SS, et al. (2009) Small molecule modulators of copper-induced Aβ aggregation. *J Am Chem Soc* 131(46):16663–16665.
18. Wu W-h, et al. (2008) Sequestration of copper from β-amyloid promotes selective lysis by cyclen-hybrid cleavage agents. *J Biol Chem* 283(46):31657–31664.
19. Porat Y, Abramowitz A, Gazit E (2006) Inhibition of amyloid fibril formation by polyphenols: Structural similarity and aromatic interactions as a common inhibition mechanism. *Chem Biol Drug Des* 67(1):27–37.
20. Ehrnhoefer DE, et al. (2008) EGCG redirects amyloidogenic polypeptides into unstructured, off-pathway oligomers. *Nat Struct Mol Biol* 15(6):558–566.
21. Bieschke J, et al. (2010) EGCG remodels mature α-synuclein and amyloid-β fibrils and reduces cellular toxicity. *Proc Natl Acad Sci USA* 107(17):7710–7715.
22. Ladiwala ARA, Dordick JS, Tessier PM (2011) Aromatic small molecules remodel toxic soluble oligomers of amyloid β through three independent pathways. *J Biol Chem* 286(5):3209–3218.
23. Lemkul JA, Bevan DR (2012) Morin inhibits the early stages of amyloid β-peptide aggregation by altering tertiary and quaternary interactions to produce "off-pathway" structures. *Biochemistry* 51(30):5990–6009.
24. Sinha S, et al. (2012) Comparison of three amyloid assembly inhibitors: The sugar *scyllo*-inositol, the polyphenol epigallocatechin gallate, and the molecular tweezer CLR01. *ACS Chem Neurosci* 3(6):451–458.
25. Lopez del Amo JM, et al. (2012) Structural properties of EGCG-induced, nontoxic Alzheimer's disease Aβ oligomers. *J Mol Biol* 421(4-5):517–524.
26. DeToma AS, Choi J-S, Braymer JJ, Lim MH (2011) Myricetin: A naturally occurring regulator of metal-induced amyloid-β aggregation and neurotoxicity. *ChemBioChem* 12(8):1198–1201.
27. Kim J, Lee HJ, Lee KW (2010) Naturally occurring phytochemicals for the prevention of Alzheimer's disease. *J Neurochem* 112(6):1415–1430.
28. Meng F, Abedini A, Plesner A, Verchere CB, Raleigh DP (2010) The flavanol (–)-epigallocatechin 3-gallate inhibits amyloid formation by islet amyloid polypeptide, disaggregates amyloid fibrils, and protects cultured cells against IAPP-induced toxicity. *Biochemistry* 49(37):8127–8133.
29. Chandrashekaran IR, Adda CG, MacRaild CA, Anders RF, Norton RS (2010) Inhibition by flavonoids of amyloid-like fibril formation by *Plasmodium falciparum* merozoite surface protein 2. *Biochemistry* 49(28):5899–5908.
30. Chandrashekaran IR, Adda CG, MacRaild CA, Anders RF, Norton RS (2011) EGCG disaggregates amyloid-like fibrils formed by *Plasmodium falciparum* merozoite surface protein 2. *Arch Biochem Biophys* 513(2):153–157.
31. Popovych N, et al. (2012) Site specific interaction of the polyphenol EGCG with the SEVI amyloid precursor peptide PAP(248-286). *J Phys Chem B* 116(11):3650–3658.
32. Pirker KF, Baratto MC, Basosi R, Goodman BA (2012) Influence of pH on the speciation of copper(II) in reactions with the green tea polyphenols, epigallocatechin gallate and gallic acid. *J Inorg Biochem* 112:10–16.
33. Sun SL, et al. (2008) Free Zn^{2+} enhances inhibitory effects of EGCG on the growth of PC-3 cells. *Mol Nutr Food Res* 52(4):465–471.
34. Cheng XR, et al. (2013) Surface plasmon resonance imaging of amyloid-β aggregation kinetics in the presence of epigallocatechin gallate and metals. *Anal Chem*, 10.1021/ac303181q.
35. Ruotolo BT, Benesch JLP, Sandercock AM, Hyung S-J, Robinson CV (2008) Ion mobility-mass spectrometry analysis of large protein complexes. *Nat Protoc* 3(7):1139–1152.
36. Bernstein SL, et al. (2009) Amyloid-β protein oligomerization and the importance of tetramers and dodecamers in the aetiology of Alzheimer's disease. *Nat Chem* 1(4): 326–331.
37. Mancino AM, Hindo SS, Kochi A, Lim MH (2009) Effects of clioquinol on metal-triggered amyloid-β aggregation revisited. *Inorg Chem* 48(20):9596–9598.
38. Suzuki Y, Brender JR, Hartman K, Ramamoorthy A, Marsh ENG (2012) Alternative pathways of human islet amyloid polypeptide aggregation distinguished by ^{19}F nuclear magnetic resonance-detected kinetics of monomer consumption. *Biochemistry* 51(41):8154–8162.
39. Ashcroft AE (2010) Mass spectrometry and the amyloid problem—how far can we go in the gas phase? *J Am Soc Mass Spectrom* 21(7):1087–1096.
40. Reinke AA, Gestwicki JE (2011) Insight into amyloid structure using chemical probes. *Chem Biol Drug Des* 77(6):399–411.
41. Larson JL, Ko E, Miranker AD (2000) Direct measurement of islet amyloid polypeptide fibrillogenesis by mass spectrometry. *Protein Sci* 9(2):427–431.
42. Hortschansky P, Schroeckh V, Christopeit T, Zandomeneghi G, Fändrich M (2005) The aggregation kinetics of Alzheimer's β-amyloid peptide is controlled by stochastic nucleation. *Protein Sci* 14(7):1753–1759.
43. Baumketner A, et al. (2006) Amyloid β-protein monomer structure: A computational and experimental study. *Protein Sci* 15(3):420–428.
44. El-Hawiet A, Kitova EN, Liu L, Klassen JS (2010) Quantifying labile protein–ligand interactions using electrospray ionization mass spectrometry. *J Am Soc Mass Spectrom* 21(11):1893–1899.
45. Wang S-H, Liu F-F, Dong X-Y, Sun Y (2010) Thermodynamic analysis of the molecular interactions between amyloid β-peptide 42 and (–)-epigallocatechin-3-gallate. *J Phys Chem B* 114(35):11576–11583.
46. Vivekanandan S, Brender JR, Lee SY, Ramamoorthy A (2011) A partially folded structure of amyloid-beta(1-40) in an aqueous environment. *Biochem Biophys Res Commun* 411(2):312–316.
47. Rauk A (2009) The chemistry of Alzheimer's disease. *Chem Soc Rev* 38(9):2698–2715.
48. Rezaei-Ghaleh N, Giller K, Becker S, Zweckstetter M (2011) Effect of zinc binding on β-amyloid structure and dynamics: Implications for Aβ aggregation. *Biophys J* 101(5): 1202–1211.
49. Faller P (2009) Copper and zinc binding to amyloid-β: Coordination, dynamics, aggregation, reactivity and metal-ion transfer. *ChemBioChem* 10(18):2837–2845.
50. Mesleh MF, Hunter JM, Shvartsburg AA, Schatz GC, Jarrold MF (1996) Structural information from ion mobility measurements: Effects of the long-range potential. *J Phys Chem* 100(40):16082–16086.
51. Shvartsburg AA, Jarrold MF (1996) An exact hard-spheres scattering model for the mobilities of polyatomic ions. *Chem Phys Lett* 261(1-2):86–91.